Increased superoxide *in vivo* accelerates age-associated muscle atrophy through mitochondrial dysfunction and neuromuscular junction degeneration

Youngmok C. Jang,[*,‡] Michael S. Lustgarten,[†,‡] Yuhong Liu,[*,‡] Florian L. Muller,[*,‡] Arunabh Bhattacharya,[*,‡] Hanyu Liang,[*,‡] Adam B. Salmon,[*,‡] Susan V. Brooks,[§] Lisa Larkin,[§] Christopher R. Hayworth,[‖] Arlan Richardson,[*,‡,¶] and Holly Van Remmen[*,‡,¶,1]

[*]Department of Cellular and Structural Biology, [†]Department of Physiology, and the [‡]Barshop Institute for Longevity and Aging Studies, University of Texas Health Science Center at San Antonio, San Antonio, Texas, USA; [§]Department of Molecular and Integrative Physiology, University of Michigan, Ann Arbor, Michigan, USA; [‖]Section of Neurobiology and Institute for Neuroscience, University of Texas, Austin, Texas, USA; and [¶]South Texas Veterans Health Care System, San Antonio, Texas, USA

ABSTRACT **Oxidative stress has been implicated in the etiology of age-related muscle loss (sarcopenia). However, the underlying mechanisms by which oxidative stress contributes to sarcopenia have not been thoroughly investigated. To directly examine the role of chronic oxidative stress *in vivo*, we used a mouse model that lacks the antioxidant enzyme CuZnSOD (*Sod1*). *Sod1*$^{-/-}$ mice are characterized by high levels of oxidative damage and an acceleration of sarcopenia. In the present study, we demonstrate that muscle atrophy in *Sod1*$^{-/-}$ mice is accompanied by a progressive decline in mitochondrial bioenergetic function and an elevation of mitochondrial generation of reactive oxygen species. In addition, *Sod1*$^{-/-}$ muscle exhibits a more rapid induction of mitochondrial-mediated apoptosis and loss of myonuclei. Furthermore, aged *Sod1*$^{-/-}$ mice show a striking increase in muscle mitochondrial content near the neuromuscular junctions (NMJs). Despite the increase in content, the function of mitochondria is significantly impaired, with increased denervated NMJs and fragmentation of acetylcholine receptors. As a consequence, contractile force in aged *Sod1*$^{-/-}$ muscles is greatly diminished. Collectively, we show that *Sod1*$^{-/-}$ mice display characteristics of normal aging muscle in an accelerated manner and propose that the superoxide-induced NMJ degeneration and mitochondrial dysfunction are potential mechanisms of sarcopenia.—Jang, Y. C., Lustgarten, M. S., Liu, Y., Muller, F. L., Bhattacharya, A., Liang, H., Salmon, A. B., Brooks, S. V., Larkin, L., Hayworth, C. R., Richardson, A., and Van Remmen, H. Increased superoxide *in vivo* accelerates age-associated muscle atrophy through mitochondrial dysfunction and neuromuscular junction degeneration. *FASEB J.* 24, 1376–1390 (2010). www.fasebj.org**

Key Words: apoptosis · oxidative stress · sarcopenia

SARCOPENIA, THE AGE-RELATED LOSS of muscle mass and function, is the major contributor to frailty in the elderly and predisposes the aging population to injuries. Despite the high occurrence and clinical relevance of sarcopenia, the exact biochemical and molecular mechanisms responsible for muscle wasting during aging are not fully understood. Reactive oxygen species (ROS) are by-products of normal cellular metabolism that can cause cellular damage by oxidation of lipids, proteins, and nucleic acids. When oxidant production increases or antioxidant defense mechanisms are impaired, the resulting state of oxidative stress can be associated with irreversible cell injury and death. Over the past few years, several researchers have proposed and reported that oxidative stress might be involved in the etiology of sarcopenia (1–2). Because mitochondria are one of the major sources of ROS and are also the primary target of oxidant-induced damage, mitochondrial abnormalities and oxidative stress have been linked together and have been a major focus in aging research with regard to the mechanisms of sarcopenia (3–4). Unlike other catabolic conditions such as cachexia or disuse that lead to muscle atrophy, sarcopenia is the result of a loss of muscle fibers, as well as a marked heterogeneity in the cross-sectional area of the remaining myofibers (5). On the basis of these observations and the postmitotic nature of skeletal muscle cells, several researchers have postulated that apoptosis may play an important role in age-related muscle loss (6–7). However, most studies describing the role of mitochondrial dysfunction, oxidative stress, and apop-

[1] Correspondence: The Sam and Ann Barshop Institute for Longevity and Aging Studies, University of Texas Health Science Center at San Antonio, 15355 Lambda Dr., San Antonio, TX 78245-3207, USA. E-mail: vanremmen@uthscsa.edu

doi: 10.1096/fj.09-146308

0892-6638/10/0024-1376 © FASEB

tosis in age-related muscle atrophy have been correlative, and direct evidence mechanistically linking these processes in sarcopenia is still lacking.

Another critical aspect underlying the mechanisms of age-related muscle loss is the dependency of myofibers on motoneuron innervation (8). A decline in the number of functional motor units and decreased innervation have been described in aged skeletal muscle (9). Other neurological changes may contribute to the development of sarcopenia, including a decrease in the number of nerve terminals, fragmentation of the neuromuscular junction (NMJ), and a decrease in neurotransmitter release (10). Mitochondria have been shown to be concentrated in the presynaptic nerve terminal, as well as in the postsynaptic endplates in muscle (11), suggesting a decline in mitochondrial bioenergetic function; hence, ROS generation may impact the regulation of synaptic transmission and potentially contribute to loss of neuromuscular junction innervation. Indeed, in a recent report by Dupuis *et al.* (12), the overexpression of uncoupling protein 1 (UCP1) in the skeletal muscle resulted in significant alterations of NMJ and triggered distal motoneuron degeneration. Furthermore, a previous study from our laboratory demonstrated that in various models of denervation (aging, ALS SOD1 mutant, *Sod1*$^{-/-}$, and surgical denervation), the extent of muscle atrophy strongly correlated with mitochondrial ROS generation (13). These data suggest a potential link between oxidative stress and mitochondrial dysfunction in maintenance of NMJ integrity. Therefore, the purpose of this study is to provide direct evidence by which chronic oxidative stress mediates muscle atrophy *in vivo* as a function of age. Using a mouse model that lacks an important antioxidant enzyme, CuZnSOD (*Sod1*), we show that chronic oxidative stress accelerates age-dependent muscle atrophy with age-associated impairment of mitochondrial bioenergetic function and a concomitant increase in mitochondrial ROS generation. Mitochondrial dysfunction occurs not only in the interfibrillar mitochondria but also in subsarcolemmal mitochondria, thereby contributing to degeneration of the NMJ and loss of innervated myofibers. Furthermore, chronic oxidative stress *in vivo* also sensitizes mitochondria to release proapoptotic factors, ultimately leading to apoptotic loss of myonuclei and contributing to muscle atrophy.

MATERIALS AND METHODS

Animals

The *Sod1*$^{-/-}$ mice have been previously described (14–15). The mice were maintained under specific pathogen-free conditions in the heterozygous (*Sod1*$^{+/-}$) state and backcrossed with C57BL/6J females (Jackson Laboratory, Bar Harbor, ME, USA) for >20 generations. In our colony, the median life span of *Sod1*$^{-/-}$ mice is ~23 mo and ~31 mo for wild-type (WT) mice. Unless noted, 18- to 22-mo-old female mice were used in the experiments. All procedures were approved by the Institutional Animal Care and Use Committee at the University of Texas Health Science Center at San Antonio and the Audie L. Murphy Veterans Hospital, San Antonio.

Histology

Gastrocnemius muscle was embedded in paraffin and sectioned (10 μm) from the midbelly, then stained with hematoxylin and then with eosin. Images were visualized and captured with Nikon Element software (Nikon Inc., Melville, NY, USA).

Fiber typing

Six-micrometer frozen sections were obtained from gastrocnemius/plantaris/soleus muscle. Sections were fixed in ice-cold 4% paraformaldehyde (PFA; pH 7.4) at 4°C for 20 min. Sections were then washed twice with PBS containing 0.1% Triton-X-100 for 10 min. Blocking was performed with PBS containing 3% BSA and 0.1% Triton-X-100 for 1 h at room temperature (RT). Primary antibodies specific for skeletal muscle myosin heavy chain (MyHC) type IIB (BFF3), type I (BAD5), and type IIA (SC-71; Sigma, St. Louis, MO, USA) were added in 1:1000 dilution in PBS and incubated for 90 min at RT. After washing sections 3 times in PBS, goat-anti-mouse Alexa 488, 594, and 680 secondary antibodies (Invitrogen, Carlsbad, CA, USA) were applied (1:250 dilution) and incubated at RT for 1 h in the dark. Sections were mounted in Vectashield with DAPI (Vector Laboratories, Burlingame, CA, USA), and images were captured using a Nikon Eclipse TE2000-U fluorescence microscope (Nikon Inc.).

Transmission electron microscopy (EM)

Muscle blocks (1 mm^3) fixed in 2% paraformaldehyde and 2.5% gluteraldehyde in 0.1 M sodium cacodylate buffer, were postfixed with 1% osmium tetroxide followed by 1% uranyl acetate. The blocks were then dehydrated through a graded series of ethanol washes and embedded in resin. Blocks were cut in ultrathin (80 nm) sections on a Reichert Ultracut UCT (Reichert, Vienna, Austria), stained with uranyl acetate followed by lead citrate and viewed on a Jeol 1230 EX transmission electron microscope (Jeol Ltd., Akishima, Japan) at 80 kV.

Immunoblot analysis

Protein extracts were separated using the standard Western blot protocol. Blots were visualized and scanned on a Typhoon 9400 (Amersham, Piscataway, NJ, USA). Quantification of the immunoblots was performed with ImageQuant Software (Sunnyvale, CA, USA).

Isolation of the skeletal muscle mitochondria

Mitochondria were purified from hindlimb muscle as previously described (1).

Superoxide release

Extramitochondrial superoxide release was measured by electron paramagnetic resonance (EPR) using the spin trap, 5-diisopropoxyphosphoryl)-5-methyl-1-pyrroline-*N*-oxide (DIPPMPO; Alexis Biochemicals, San Diego, CA, USA). DIPPMPO forms an adduct with superoxide, resulting in the generation of DIPPMPO-OOH. EPR measurements were performed using an X-band MS200 spectrometer (Magnetech, Berlin, Germany). Mito-

chondria (1 mg/ml) were incubated at 37°C with or without glutamate and malate and DIPPMPO (50 mM) for 30 min in 125 mM KCl, 10 mM MOPS, 2 mM diethylene triamine pentaacetic acid, 5 mM $MgCl_2$, and 2 mM K_2HPO_4, pH 7.44. For measurements, 40 μl of sample was transferred to 50-μl capillary tubes and measured at RT with the following settings: receiver gain, 5×10^5; microwave power, 20 mW; microwave frequency, 9.55 GHz; modulation amplitude, 2 *G*; scan time, 40 s; and scan width, 100 *G*, with an accumulation of 10 scans.

Mitochondrial H_2O_2 generation

The rate of mitochondrial H_2O_2 production was measured using the Amplex Red-horseradish peroxidase method, as previously described (16–17). Fluorescence was followed at an excitation wavelength of 545 nm and emission wavelength of 590 nm; then it was converted to the rate of H_2O_2 production using a standard curve. The reaction buffer consisted of 125 mM KCl, 10 mM HEPES, 5 mM $MgCl_2$, and 2 mM K_2HPO_4, pH 7.44.

ATP production

The rate of ATP production by mitochondria was measured measured using a luciferase/luciferin-based system (ATP Bioluminescence Assay Kit CLS II; Roche Molecular Biochemicals, Indianapolis, IN, USA), as previously described (1).

Mitochondrial respiration

Mitochondrial oxygen consumption was measured using a Clark electrode system (Hansatech Instruments Ltd., Norfolk, UK), as previously described (13). The respiratory buffer consisted of 125 mM KCl, 10 mM HEPES, 5 mM $MgCl_2$, and 2 mM K_2HPO_4, pH 7.44, with 0.3% BSA. State 3 respiration was induced with the addition of 0.3 mM ADP.

Treadmill endurance capacity test

Mice were run on an Exer-6 treadmill (Columbus Instruments, Columbus, OH, USA) on a 15% incline. The first 5 min were considered as exercise acclimatization, as mice were run at 7 m/min for 5 min. Mice were then run at a speed of 12 m/min until 120 min. Speed was increased to 17 m/min for 10 min if an animal reached 120 min. The speed was increased to 22 m/min until exhaustion. Exhaustion was determined by a failure to engage the treadmill in the presence of repetitive shocks.

Measurement of biochemical metabolites during treadmill exercise

The mouse tail was nicked with a scalpel, and the tail vein was massaged to obtain an appropriate volume of blood (~5 μl) for both glucose and lactate measurements. Blood glucose was measured using the OneTouch Ultra blood glucose meter (Lifescan, Milpitas, CA, USA). Blood lactate was measured using the Lactate Plus meter (Nova Biomedical, Waltham, MA, USA). Measurements of glucose and lactate levels during exercise were performed at the indicated time point (*i.e.*, at 0, 20, and 40 min of running, and at exhaustion) *via* use of the glucose or lactate meter, respectively.

Mitochondrial permeability transition pore (PTP) opening and mitochondrial proapoptotic protein release assay

The rate of PTP opening was measured in mitochondria using protocols previously described (18). Briefly, mitochondrial swelling was measured by the decrease in absorbance at 520 nm using a spectrophotometer. Cytochrome *c* and apoptosis-inducing factor (AIF) release were measured by Western blot analyses in the supernatant (released) and pellet (intact) after 1 h incubation at 37°C with different doses of Ca^{2+}.

Cell-free apoptosis

Cell-free apoptosis was measured using protocols previously described, with slight modification (19). Mouse liver nuclei were purified by a sucrose gradient as previously described (20). To perform cell-free apoptosis, three extracts (skeletal muscle cytosol, liver nuclei, and freshly isolated muscle mitochondria) were mixed; supplemented with an ATP-regenerating system comprising 10 mM phosphocreatine, 2 mM ATP, and 150 μg/ml creatine phosphokinase; and incubated at 37°C. After 4 h of incubation, nuclei were stained with Hoescht and visualized under a fluorescent microscope. The number of apoptotic nuclei, identified by chromatin condensation, nuclear fragmentation, and blebbing, were determined in 20 random fields for each animal (n=3 WT and n=4 *Sod1*$^{-/-}$). Data were expressed as the ratio of apoptotic nuclei per total number of nuclei in all fields.

Apoptosis assessed by DNA fragmentation

DNA fragmentation was quantified by cytosolic mononucleosomes and oligonucleosomes (180-bp nucleotides or multiples) using a Cell Death ELISA kit (Roche) and peroxidase *in situ* oligo ligation (ISOL) assay kit (Chemicon/Millipore, Billerica, MA). For cell-death ELISA, muscle lysates were used (n=6), and all samples were measured in triplicate. For ISOL, paraffin-embedded sections from 20-mo gastrocnemius muscle were used (n=3). Procedures were performed according to the manufacturer's protocol.

Caspase-3 activity

Caspase-3 activity was measured using the synthetic peptide *N*-acetyl-DEVD-AMC (BD PharMingen, San Diego, CA, USA). Cleavage of the AMC and its fluorescence were measured on a spectrofluorometer at 380 nm excitation and 440 nm emission. All samples were measured in triplicate.

Single-fiber analyses

Single fibers were isolated, and fiber size and myonuclear number were measured as described by Wada *et al.* (21–22). Briefly, skinned gastrocnemius or tibialis anterior muscle was clamped to minimize fiber length variability and fixed in 4% paraformaldehyde (PFA) for 2 d at RT. Small bundles of fibers were dissected, incubated in 40% NaOH for 2 h, and agitated vigorously for 20 min. Released fibers were washed in PBS and stained with 10 μM DAPI, and images of 25–45 single fibers/animal were captured with a Nikon Eclipse TE2000 with ×20 objective. Fiber diameter was measured at 10 locations over ≥500 μm of fiber, and all nuclei were counted using Nikon Element software. Myonuclear domain was measured by fiber volume/number of nuclei (fiber segment length × πr^2/nuclei).

Immunohistochemistry of NMJs

Immunofluorescence images of NMJs were prepared as described by Schaefer *et al.* (23). For details, see Supplemental Data.

Isometric contraction protocol

Isometric contractile properties were measured *in situ* in gastrocnemius muscle. See Supplemental Data for details.

Statistics

Results are expressed as means ± SE. Significance was established using Student's *t* test and ANOVA when appropriate. Differences were considered significant at $P < 0.05$. Two-way ANOVA with Bonferroni *post hoc* test were used when comparing age and genotype differences.

RESULTS

Age-dependent loss of muscle mass in *Sod1*$^{-/-}$ mice

Gross morphology was compared between WT and *Sod1*$^{-/-}$ mice at various ages. On visual analysis, overall loss of hindlimb muscle mass was clearly evident in *Sod1*$^{-/-}$ mice, and by 20 mo of age, the wet weight of the gastrocnemius muscle was ~40% less than that of the age-matched WT littermates (**Fig. 1*A, B***). The gastrocnemius muscle, which is composed of predominantly type IIb fast fibers in mice (24), was most affected by loss of CuZnSOD, and atrophy was exacerbated drastically with age in the *Sod1*$^{-/-}$ mice (Fig. 1*A, B*). Next, in order to determine whether the decrease in muscle mass was the result of actual myofiber atrophy, transverse sections of gastrocnemius obtained

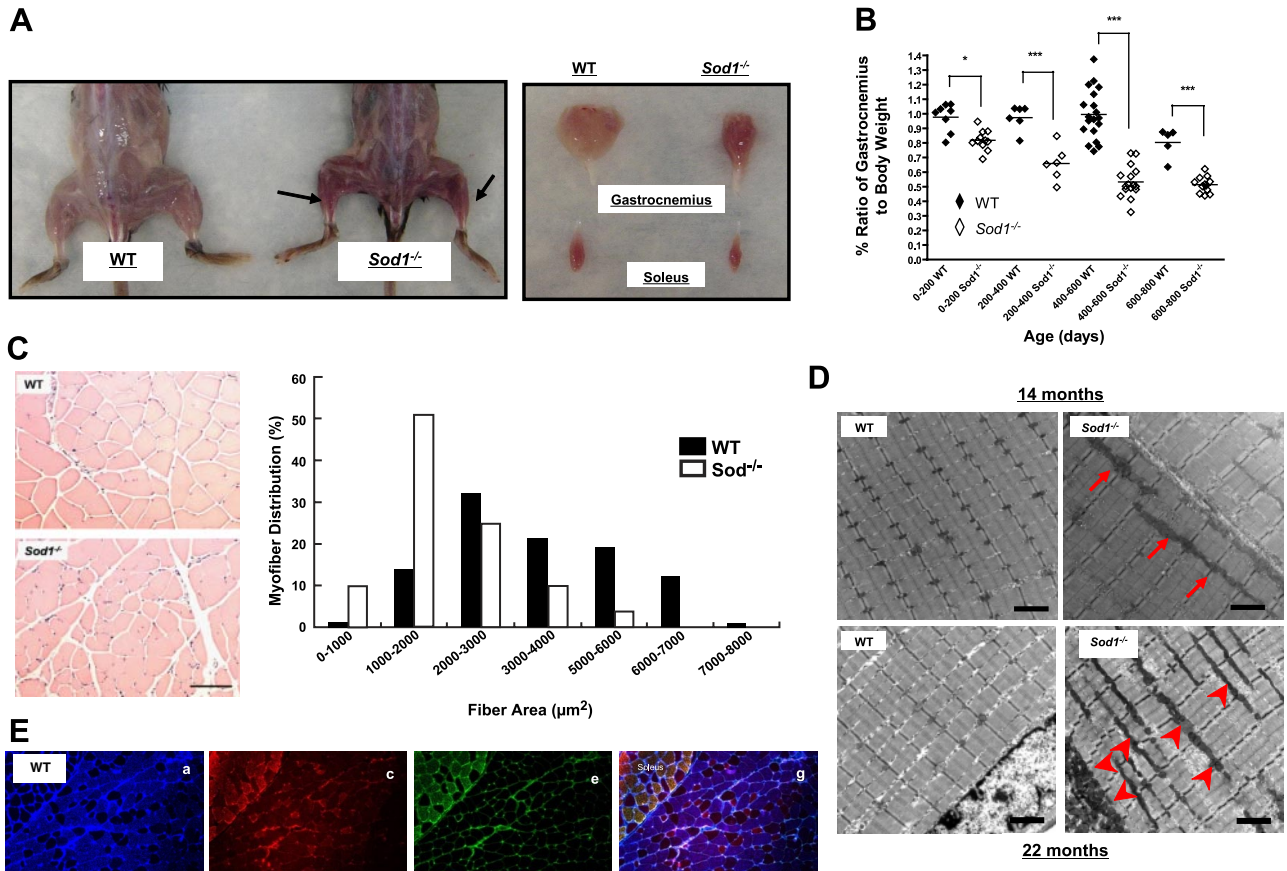

Figure 1. Age-dependent loss of muscle mass corresponds to increased mitochondria content and oxidative fibers in *Sod1*$^{-/-}$ mice. *A*) Left panel: gross morphology of skinned hindlimb muscles of 20-mo-old *Sod1*$^{-/-}$ and WT mice. Right panel: comparison of individual muscles. *B*) Comparison of age-associated changes in wet weight of gastrocnemius mass normalized to body weight. *C*) Top panels: gastrocnemius cross section at 20 mo of age from hematoxylin and eosin stain. Bottom panel: frequency distribution of fiber cross-sectional area (μm^2) of gastrocnemius muscle in WT and *Sod1*$^{-/-}$ at 20 mo (n=4). *D*) EM images of gastrocnemius at 14 mo (top panels) and at 22 mo (bottom panels). Arrows and arrowheads indicate increased mitochondria. *E*) Immunofluorescence images of muscle fiber types from WT (*a, c, e, g*) and *Sod1*$^{-/-}$ (*b, d, f, h*) gastrocnemius muscle at 20 mo. *a, b*) Type IIb (blue). *c, d*) Type IIa (red). *e, f*) Type I (green). *g, h*) Merged images. Scale bars = 50 μm (*C*); 2 μm (*D*); 100 μm (*E*).

from age-matched *Sod1*$^{-/-}$ and WT mice were compared (Fig. 1*C*). Quantitative analysis of individual fiber cross-sectional areas revealed that the myofiber size distribution shifted to the left in *Sod1*$^{-/-}$, suggesting that smaller fibers are more prevalent in muscle of *Sod1*$^{-/-}$ mice. Moreover, muscle of *Sod1*$^{-/-}$ mice appears to be darker (redder) in color than muscle from age-matched WT mice (Fig. 1*B*). Indeed, as illustrated in Fig. 1*E*, a selective loss of white/fast glycolytic fibers (type IIb) or the conversion to either fast oxidative (type IIa) or slow fibers (type I) was evident in muscle from *Sod1*$^{-/-}$ mice. In support of these observations, we found a significant up-regulation of proteins normally abundant in slow fibers (myoglobin and troponin I slow) in muscle from *Sod1*$^{-/-}$ mice at 20 mo of age (Supplemental Fig. S2). We further examined the ultrastructure of muscle fibers using transmission EM. At 14 mo of age, WT and *Sod1*$^{-/-}$ myofibrils looked similar in size and appeared normal. However, by 22 mo of age, myofibrils and the contractile apparatus from the muscle of *Sod1*$^{-/-}$ mice were visibly disorganized and much smaller in size. In addition, mitochondria from muscle of *Sod1*$^{-/-}$ were abnormally shaped and larger compared to mitochondria in muscle from age-matched WT. Furthermore, mitochondria from muscle of *Sod1*$^{-/-}$ were often clustered in longitudinal rows along the myofibrils. At 22 mo of age, mitochondria from muscle of *Sod1*$^{-/-}$ mice displayed a striking increase in both subsarcolemmal (SSM) and interfibrillar mitochondria (IFM) compared to muscle from WT (Fig. 1*D*).

Age-associated increase in mitochondrial ROS generation and mitochondrial dysfunction in *Sod1*$^{-/-}$ muscle

To test whether a proliferation in mitochondria content affected mitochondrial function, we assessed mitochondrial respiration, rate of ATP production, and mitochondrial ROS emission using isolated mitochondria preparation from the hindlimb muscles. To evaluate the mitochondrial bioenergetic function, we examined the mitochondria respiratory control ratio (RCR) by measuring state 3 and state 4 oxygen consumption and the rate of ATP production from the isolated mitochondria. In muscle mitochondria from young mice, there were no statistical differences in either RCR or ATP (data not shown). However, with age, the muscle mitochondria from *Sod1*$^{-/-}$ mice showed an ~30% decline in the RCR, indicating that muscle mitochondria from *Sod1*$^{-/-}$ mice are uncoupled. As a consequence, ATP production in *Sod1*$^{-/-}$ mitochondria is reduced to 25% of WT levels at 20 mo of age. Next, in order to gain insight on whether the decline in mitochondrial function in *Sod1*$^{-/-}$ leads to generation of mitochondrial ROS, we compared the levels of superoxide ($O_2^{\cdot -}$) and hydrogen peroxide (H_2O_2) generation between the isolated mitochondria from *Sod1*$^{-/-}$ and WT mice. Although, CuZnSOD is mostly located in the cytosolic compartment, a small portion of CuZnSOD is located in the intermembrane space of mitochondria to scavenge $O_2^{\cdot -}$ generated toward the cytoplasm by complex III (17, 25). Therefore, we tested the possibility of whether the lack of *Sod1* resulted in increased levels of extramitochondrial $O_2^{\cdot -}$ using EPR with the spin-trap probe, 5-diisopropoxyphosphoryl)-5-methyl-1-pyrroline-*N*-oxide (DIPPMPO) in the presence of complex I-linked substrate (glutamate/malate). As shown in **Fig. 2*A***, isolated mitochondria from *Sod1*$^{-/-}$ muscle released significantly higher levels of $O_2^{\cdot -}$ compared to WT muscle mitochondria. We also assessed the levels of H_2O_2 emission from the isolated mitochondria at 20 mo of age. In state 1, when mitochondria are respiring on their endogenous substrates, H_2O_2 production was increased by ~3-fold in mitochondria from *Sod1*$^{-/-}$ compared to age-matched WT mice. Likewise, when mitochondrial respiration was stimulated with the complex I-linked substrates, glutamate and malate, we found a comparable increase in mitochondrial H_2O_2 generation in the *Sod1*$^{-/-}$ mice. Despite the observation that a lack of CuZnSOD leads to a dramatic increase in the mitochondrial release of ROS and oxidative damage, we found no compensatory up-regulation of other major antioxidant enzymes in the mitochondria or in the cytosolic compartment (Supplemental Fig. S3).

Skeletal muscle mitochondria and their oxidative capacity is a crucial factor in determining overall endurance and fatigue (26). Thus, we analyzed whether increased ROS and the decline in mitochondrial function affect the endurance exercise performance in these animals. *Sod1*$^{-/-}$ and WT mice at 12–14 mo of age were run on a motorized treadmill until the animals reached exhaustion (n=8–10). As shown in Fig. 2*E*, *Sod1*$^{-/-}$ mice show a significant decrease in running distance and work compared to WT mice (859±76 *vs.* 303±95 m). This suggests that the overall oxidative capacity is significantly decreased in *Sod1*$^{-/-}$ mice, possibly due to an inability of mitochondria to generate ATP. Furthermore, when plasma glucose and plasma lactate levels were compared following exercise (Fig. 2*F, G*, respectively), *Sod1*$^{-/-}$ mice exhibited a higher level of lactate and significantly lower levels of plasma glucose compared to WT mice, suggesting that oxidative metabolism might be altered in the skeletal muscle from *Sod1*$^{-/-}$ mice during high-energy-demanding conditions.

Increased mitochondrial permeability transition and elevated apoptotic potential in muscle mitochondria from *Sod1*$^{-/-}$ mice

It is well documented that mitochondrial ROS and oxidative stress are potent triggers in the intrinsic pathway of the apoptotic cascade (27). Thus, we tested whether the mitochondrial dysfunction and increased ROS generation seen in *Sod1*$^{-/-}$ muscle lead to mitochondrial-mediated apoptosis. First, to test mitochondrial outer membrane integrity, we measured cytochrome *c* oxidase activity in the presence and absence of the detergent, *N*-dodecyl-β-D-maltoside. Our results showed that 85–90% of the mitochondria were free of

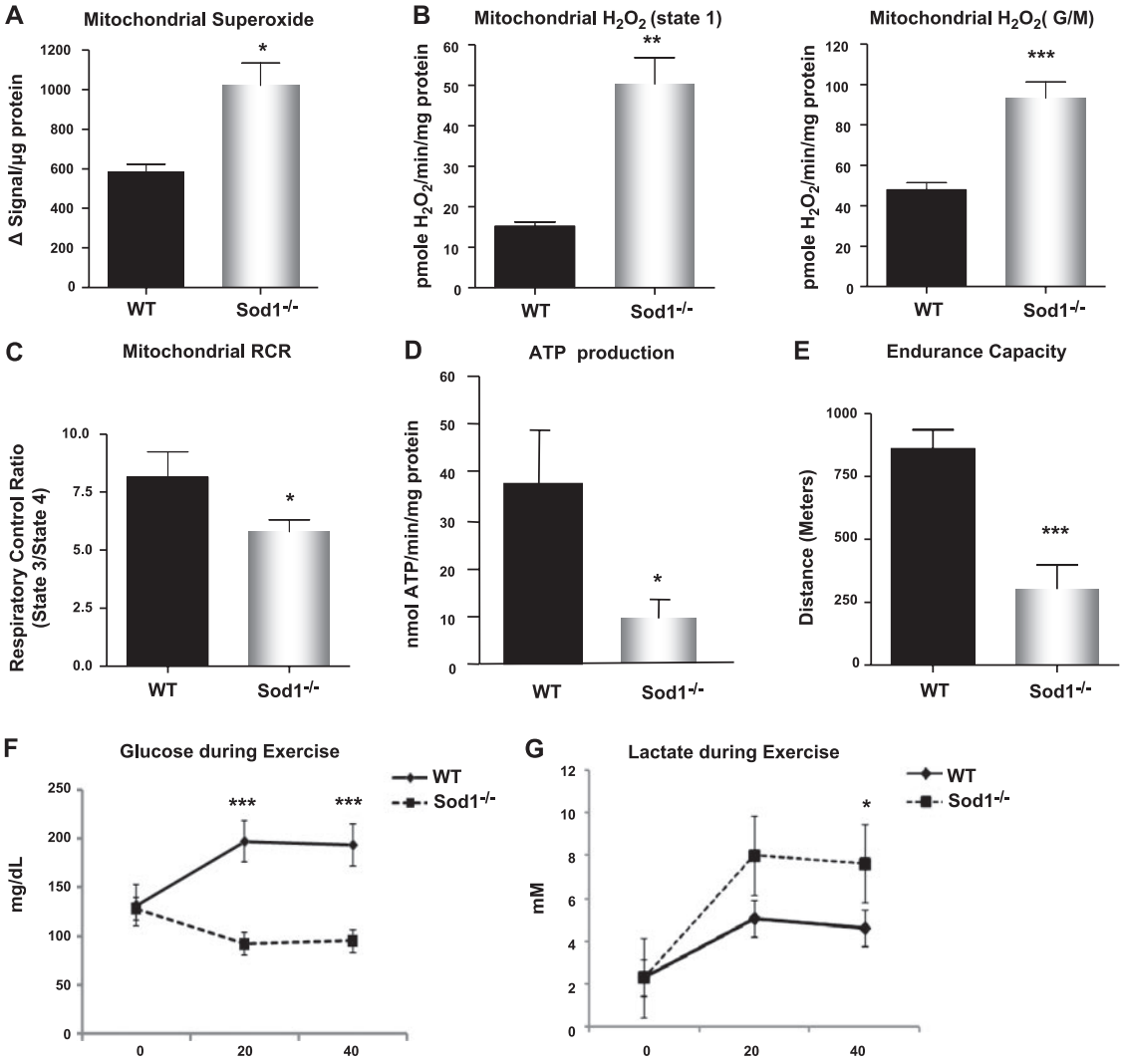

Figure 2. Mitochondrial dysfunction and increased ROS generation in aged *Sod1*$^{-/-}$ mice. *A*) Extramitochondrial superoxide generation in isolated mitochondria, measured using EPR. Succinate was used as substrate. *B*) Rate of mitochondrial H_2O_2 production measured using amplex red in state 1 (left panel) and in response to complex I-linked substrate, glutamate, and malate (right panel). *C*) Mitochondrial oxygen consumption, expressed as RCR. *D*) Rate of ATP generation in isolated mitochondria at 20 mo (n=6). *E*) Treadmill endurance test (run to exhaustion) results from 12- to 14-mo-old WT and *Sod1*$^{-/-}$ mice. (n=8–10) *F*, *G*) Plasma glucose (*F*) and plasma lactate (*G*) levels measured immediately following exercise. Values are means ± SE. *$P < 0.05$; **$P < 0.01$; ***$P < 0.001$.

outer membrane damage (Supplemental Fig. S4). Next, we examined the sensitivity of the PTP opening by Ca^{2+} in mitochondria from WT and *Sod1*$^{-/-}$ mice at 20 mo of age. As illustrated in **Fig. 3*A***, the mitochondrial swelling was significantly greater in the mitochondria from the *Sod1*$^{-/-}$compared to the age-matched WT mice. Furthermore, Ca^{2+} retention capacity was significantly reduced in mitochondria isolated from *Sod1*$^{-/-}$ muscle (Fig. 3*B*). To test whether mitochondrial PTP opening kinetics were influenced by its composition, we measured protein levels of the voltage-dependent anion channel (VDAC), cyclophilin D (CypD), and adenine nucleotide translocator (ANT), three integral constituents of the mitochondrial PTP. The levels of these proteins did not change with either age or *Sod1* deficiency (Supplemental Fig. S5), suggesting that other factors are involved in the sensitivity of the pore opening. The opening of the PTP leads to release of proapoptotic proteins from the mitochondrial intermembrane space. When the PTP was activated by increasing concentrations of Ca^{2+}, mitochondria from the *Sod1*$^{-/-}$ muscle showed a significant elevation in cytochrome *c* release. Similarly, AIF, a proapoptotic protein that initiates apoptosis in a caspase-independent manner, showed a significant increase after PTP was triggered by Ca^{2+} (Fig. 3*B*). In addition to the involvement of the mitochondrial PTP in initiating apoptosis, the Bcl-2 family proteins also play a crucial role in regulating mitochondrial apoptosis. The Bcl-2 family proteins can act directly on the outer membrane of mitochondria and either inhibit or induce the release of proapoptotic factors from the mitochondria. Therefore, we analyzed whether levels of key multidomain Bcl-2 family proteins change in mus-

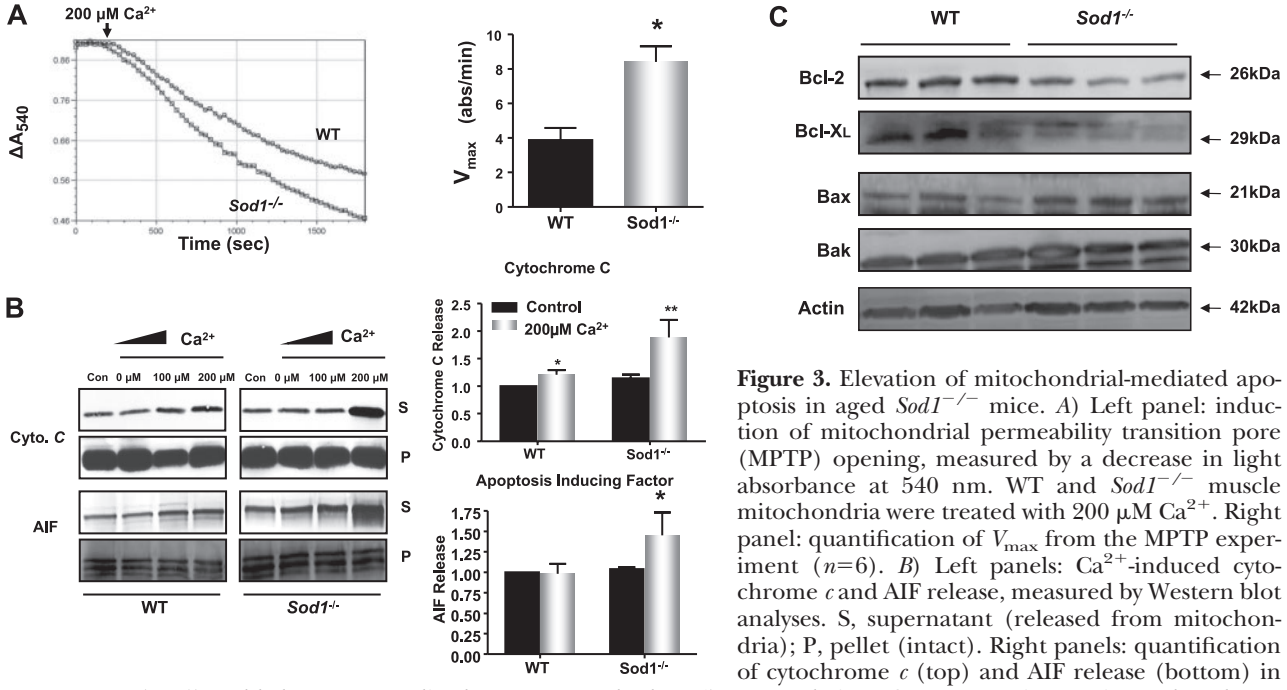

Figure 3. Elevation of mitochondrial-mediated apoptosis in aged *Sod1*$^{-/-}$ mice. *A*) Left panel: induction of mitochondrial permeability transition pore (MPTP) opening, measured by a decrease in light absorbance at 540 nm. WT and *Sod1*$^{-/-}$ muscle mitochondria were treated with 200 μM Ca^{2+}. Right panel: quantification of V_{max} from the MPTP experiment (n=6). *B*) Left panels: Ca^{2+}-induced cytochrome *c* and AIF release, measured by Western blot analyses. S, supernatant (released from mitochondria); P, pellet (intact). Right panels: quantification of cytochrome *c* (top) and AIF release (bottom) in supernatant (n=6). Fold change normalized to WT control value. *C*) Up-regulation of proapoptotic proteins, Bak and Bax, and down-regulation of antiapoptotic proteins, Bcl-2 and Bcl-X_L, measured by Western blot analyses. Actin was used as a loading control for each protein; one representative blot is shown.

cle from the *Sod1*$^{-/-}$ mice. Protein expression of the proapoptotic proteins, Bax and Bak, were significantly elevated in mitochondria from *Sod1*$^{-/-}$ mice, whereas the antiapoptotic proteins, Bcl-2 and Bcl-X_L, were significantly decreased, by 25 and 50%, respectively (Fig. 3*D*). Taken together, our data demonstrate that increased ROS generation and mitochondrial dysfunction in mitochondria from the *Sod1*$^{-/-}$ muscle are correlated with enhanced sensitivity to mitochondria-mediated apoptosis.

Increased apoptotic nuclei and caspase-3 activity in *Sod1*$^{-/-}$

To firmly establish the connection between the mitochondrial dysfunction seen in muscle mitochondria from the *Sod1*$^{-/-}$ mice and the susceptibility to mitochondria-mediated loss of nuclei in *Sod1*$^{-/-}$ muscle, we utilized the cell-free system to analyze the apoptotic morphology (19–20). As illustrated in **Fig. 4*A***, the nuclei incubated with mitochondria from *Sod1*$^{-/-}$ muscle showed a significant increase in number of nuclei with apoptotic features, such as blebbing, compared to fractions incubated with mitochondria from WT muscle. This result provides additional validation of our results that mitochondria from *Sod1*$^{-/-}$ are more vulnerable to the initiation of apoptosis. To further demonstrate that loss of CuZnSOD leads to an increase in apoptosis, we then measured the downstream effector, caspase-3, and DNA fragmentation in muscle lysates from *Sod1*$^{-/-}$ mice. As expected, we found a significant increase in caspase-3 activity, as well as an increase in DNA fragmentation measured by histone-complexed DNA fragment ELISA and peroxidase ISOL assay in *Sod1*$^{-/-}$ mice (Fig. 4*B*, *C* and Supplemental Fig. S6). Furthermore, EM analyses also revealed that at 20 mo of age, *Sod1*$^{-/-}$ gastrocnemius muscle shows a significant increase in myonuclei with apoptotic features, such as membrane invagination and chromatin condensation (Fig. 4*D*). Interestingly, these apoptotic nuclei are surrounded by abnormal mitochondria, which further supports our observations that oxidative stress-induced mitochondrial dysfunction greatly leads to apoptotsis.

Decrease in myonuclei number and fiber size but no change in myonuclear domain

Distinct from other cell types, skeletal muscle cells are multinucleated. Hence, the elimination of the nucleus does not follow the death of the entire cell as in mononucleated cells (28). Moreover, studies indicate that within the individual muscle fiber, not all nuclei are transcriptionally equivalent, and each nucleus governs the surrounding cytoplasmic area, called the myonuclear domain (28). To elucidate whether the increase in apoptotic signaling in muscle from *Sod1*$^{-/-}$ mice leads to deletion of myonuclei and thus increases the cytoplasmic volume per nucleus, we analyzed the number of nuclei and myonuclear domain in single fibers from the gastrocnemius muscle at 20 mo of age (**Fig. 5*A***). Consistent with reduced muscle mass, the average diameter of single fibers isolated from *Sod1*$^{-/-}$ muscle was ~10% less than WT muscle (Fig. 5*A*, *C*). In addition, in an agreement with the elevated apoptosis, the number of myonuclei (counted randomly per 500 μm length) showed a significant decrease in *Sod1*$^{-/-}$ muscle (Fig. 5*A*, *B*). Since both the fiber diameter and

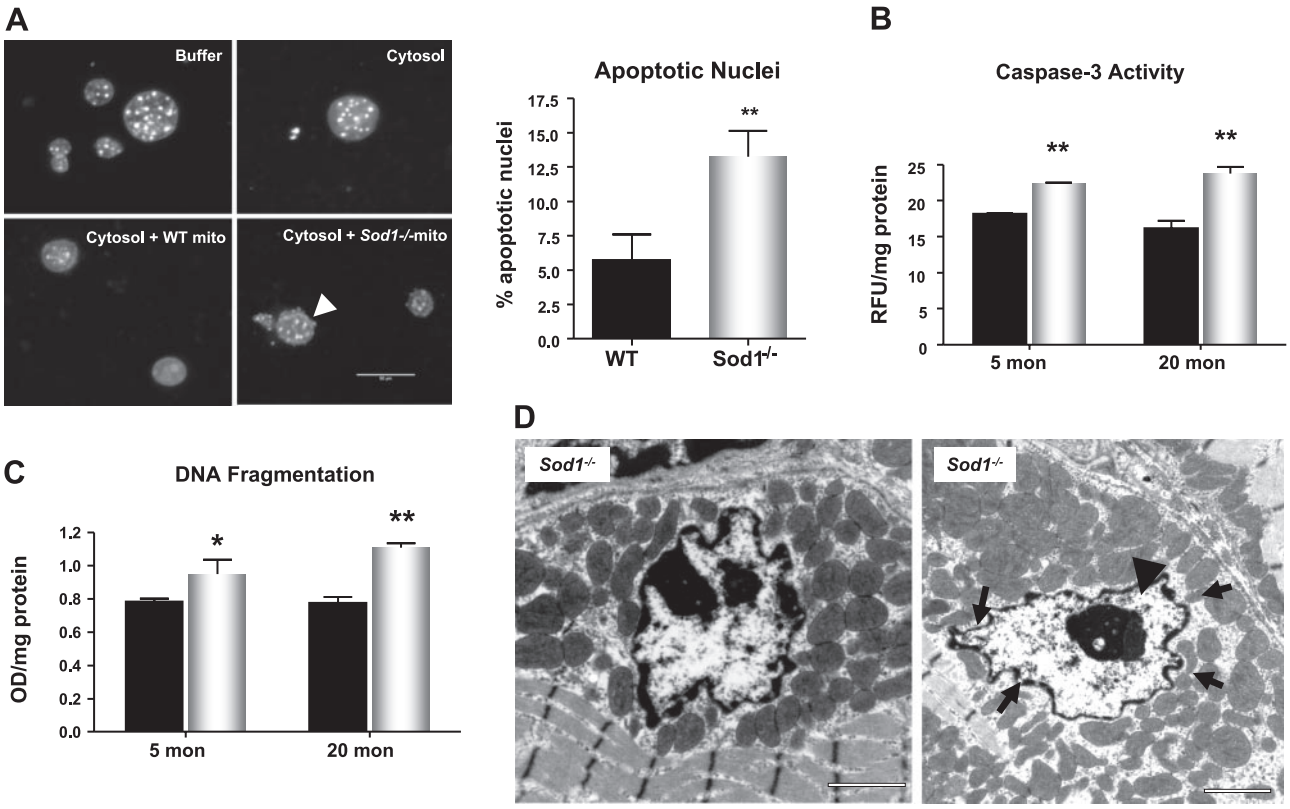

Figure 4. Elevation of caspase-3 activity and apoptosis in aged *Sod1*$^{-/-}$ mice. *A*) Left panels: cell-free apoptosis, measured by liver nuclei treated with buffer alone (top left), WT muscle cytosolic fraction alone (top right), WT mitochondria and WT cytosol (bottom left), and *Sod1*$^{-/-}$ mitochondria and *Sod1*$^{-/-}$ cytosol (bottom right). Arrowhead indicates nuclear blebbing. Right panel: quantification of apoptotic nuclei, measured 4 h after incubation. Assay was run in duplicates and repeated with mitochondria isolated from different animals (n=4). *B*) Caspase-3 activity, measured by cleavage of synthetic peptide *N*-acetyl-DEVD-AMC (n=6). *C*) Apoptosis, determined by quantification of DNA fragmentation (mononucleosome and oligonucleosome) (n=6). Values are means ± SE. *$P < 0.05$; **$P < 0.01$. *D*) EM images of myonuclei undergoing apoptotic changes. Arrows indicate nuclear membrane invagination; arrowhead indicates chromatin condensation. Scale bars = 2 μm.

the number of nuclei decreased, the mean value of myonuclear domain (cytoplasmic volume/nuclei) did not show any difference between the muscle from WT mice and that from the *Sod1*$^{-/-}$ mice (Fig. 5*D*). However, it is noteworthy that in fibers from *Sod1*$^{-/-}$ mice, several myonuclei were clumped together, and in some cytoplasmic areas, the nuclei were absent and unevenly distributed (Fig. 5*A*, arrows). Furthermore, on close examination by EM, some fibers from *Sod1*$^{-/-}$ mice exhibited a complete degeneration, with necrotic features of an altered mitochondrial structure, an accumulation of lipid vacuoles, and a dramatic loss of myofibrillar proteins, while juxtaposing myofibers appeared normal (Fig. 5*E*). Collectively, these results demonstrate that increased apoptotic deletion of myonuclei was greater in muscle from *Sod1*$^{-/-}$ compared with WT mice, and as a consequence, the size of the individual fibers are decreased. However, apoptotic/necrotic degeneration and atrophy may occur on a fiber-to-fiber basis, and not necessarily alter neighboring fibers.

Alteration of NMJ and impaired contractility in *Sod1*$^{-/-}$ muscle

Sod1$^{-/-}$ mice on a mixed CD1/129 genetic background were previously reported to have alterations in the structure of NMJs, muscle fiber type grouping, and a slow progressive loss of neurons in the lower legs that was classified as a distal axonopathy (29–30). Given that muscle atrophy and muscle fiber degeneration in *Sod1*$^{-/-}$ muscle occur in a fiber-by-fiber fashion, and a decline in innervation and loss of motor units are known to be important endogenous causes of sarcopenia, we tested whether denervation plays a role in the age-associated atrophic process. We first examined the ultrastructure of NMJs by EM at 20 mo. As illustrated in Fig. 5*A*, we found that in muscle from *Sod1*$^{-/-}$, NMJs have structural aberrations that are not evident in WT mice. The convoluted folding structure of the synaptic cleft is clearly reduced in the NMJs from *Sod1*$^{-/-}$ mice, and the synaptic vesicles observed in WT are lower in NMJs from *Sod1*$^{-/-}$ mice (n=4). This abnormality in NMJ structure may be the hallmark of a denervated NMJ commonly observed in aging skeletal muscle. But more strikingly, there is a dramatic increase in mitochondria surrounding the NMJ. Mitochondria near the NMJ in *Sod1*$^{-/-}$ muscle appear to be dilated and structurally abnormal similar to that seen in IFM of *Sod1*$^{-/-}$muscle (**Fig. 6*A***). To test whether mitochondrial function in mitochondria located near the NMJ is compromised in muscle from *Sod1*$^{-/-}$ mice, we isolated only the SSM

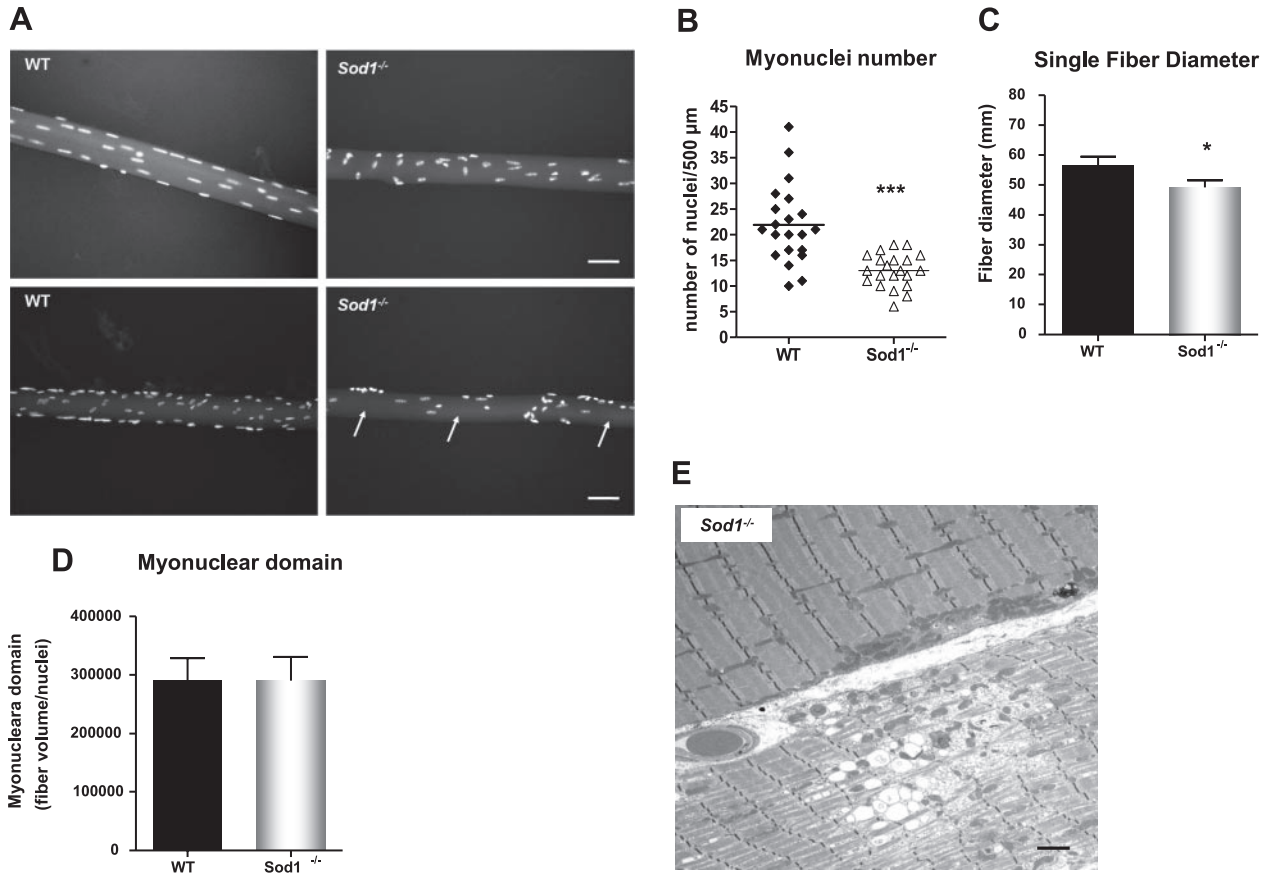

Figure 5. Aged *Sod1*$^{-/-}$ mice exhibit decreases in myonuclei number and fiber diameter. *A*) Single-fiber size comparison of WT and *Sod1*$^{-/-}$ gastrocnemius muscle at 20 mo. Arrows indicate areas lacking myonuclei. *B*) Quantification of myonuclei per 500 μm in both WT and *Sod1*$^{-/-}$ gastrocnemius muscle at 20 mo. *C*) Quantification of average fiber diameter across single fibers in gastrocnemius muscle from WT and *Sod1*$^{-/-}$ mice at 20 mo. *D*) Quantification of myonuclear domain, measured by fiber volume per myonuclei number. *E*) EM of fibers showing dystrophic/necrotic fiber in *Sod1*$^{-/-}$ muscle at 20 mo. Black arrows indicate abnormal mitochondria; arrowheads indicate lipid vacuoles. Scale bars = 50 μm (*A*); 2 μm (*E*). Values are means ± SE. $^{*}P < 0.05$; $^{***}P < 0.001$.

population of mitochondria, as opposed to the total mitochondrial population used in our previous experiments. We found that in SSM in *Sod1*$^{-/-}$ muscle, RCR was significantly decreased by 40%, and the ATP production was diminished by 80% at 20 mo. Moreover, SSM from *Sod1*$^{-/-}$ muscle showed a pronounced increase in H_2O_2 emission (Fig. 6*B*). On the basis of these data, we postulate that the function of many NMJs may be compromised as a result of mitochondrial dysfunction and oxidative damage at the NMJ, potentially contributing to loss of innervation. However, it is important to note that the SSM population of mitochondria also contains subsarcolemmal mitochondria not associated with the NMJ. Alterations in function of these non-NMJ associated mitochondria may also have implications for alterations in synaptic transmission, ion exchange, action potential propagation, or other membrane cell signaling processes.

To establish whether denervation is elevated with age in muscle from *Sod1*$^{-/-}$ mice, the innervation state of NMJs was analyzed by an immunofluorescent staining technique. When innervated, endplates and nerve terminal overlay each other; thus, the innervation state can be quantified by measuring the percentage of overlaid NMJs. Motor endplates were identified with fluorophor-conjugated α-bungarotoxin, which stains the α subunit of acetylcholine receptors (AChRs), and peripheral motor axons were identified by crossing WT and *Sod1*$^{-/-}$ mice with *Thy1* EYFP transgenic mice previously described (31). As shown in Fig. 6*C*, *D*, a histological examination of NMJs in *Sod1*$^{-/-}$ at 18–20 mo demonstrates marked alterations in NMJs compared to age-matched WT NMJs. Preterminal portions of motor axons exhibit regions of abnormal thinning, distension, and sprouting. In the postsynaptic endplate, contrary to the pretzel-like shape of WT endplates, *Sod1*$^{-/-}$ endplates are dispersed and extensively fragmented. In the muscle of *Sod1*$^{-/-}$, alterations in NMJs were observed scarcely as early as ~5 mo and progressively increased with age (Fig. 6*D*). By 18 mo of age, 78% of NMJs were completely denervated, and 18% were partially denervated in *Sod1*$^{-/-}$, whereas in WT, denervated NMJs were undetectable, and only 6% were partially innervated (Fig. 6*D*). In senescent (30 mo) WT mice, the extent of denervation is also increased, to an extent similar to that of 18- to 20-mo-old *Sod1*$^{-/-}$ mice (data not shown). Because muscle fibers are heterogeneous and age-related muscle atrophy in *Sod1*$^{-/-}$ ap-

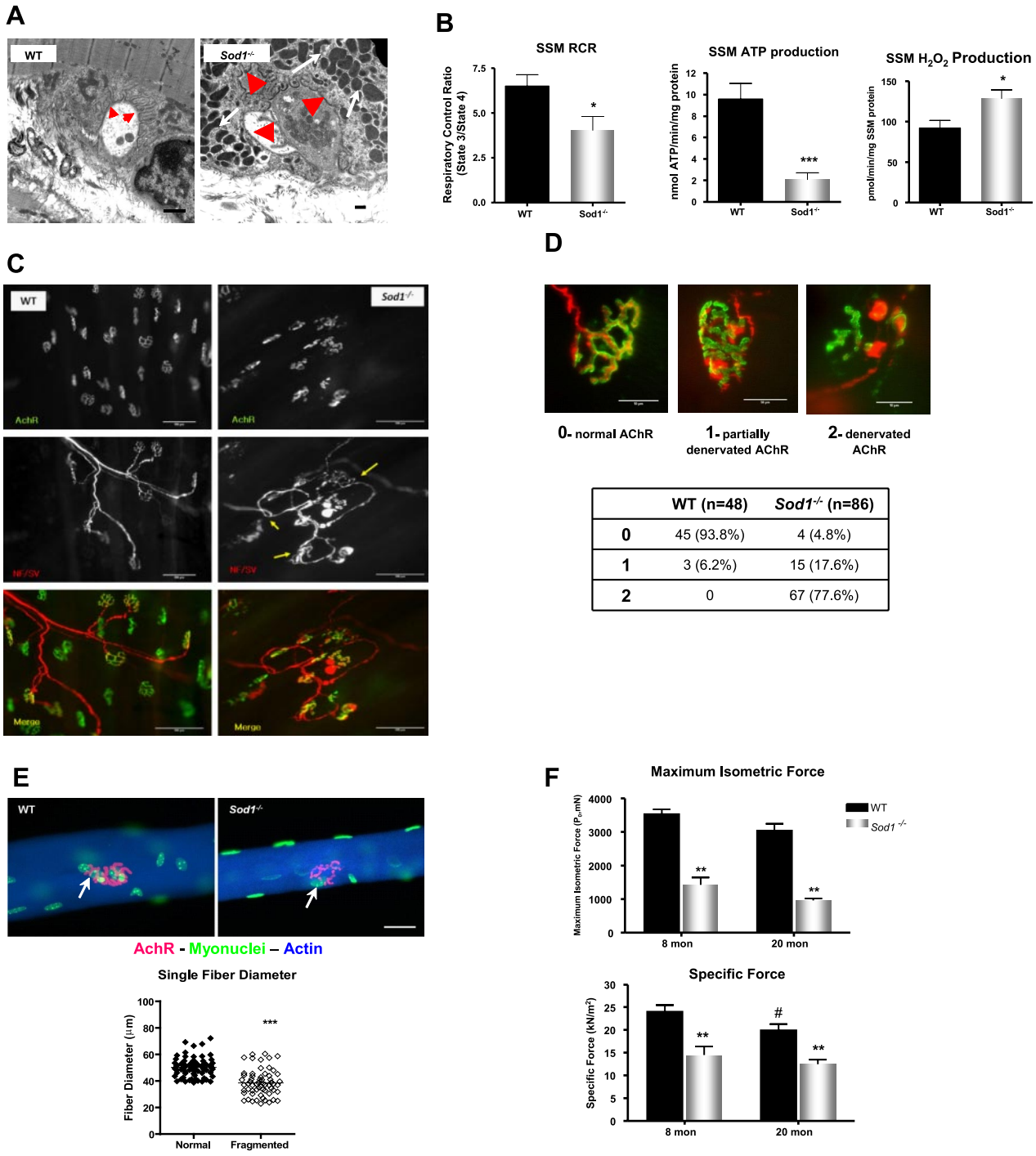

Figure 6. Aged *Sod1*$^{-/-}$ mice exhibit alterations in NMJs and increased denervation. *A*) EM analysis of NMJ of gastrocnemius at 20 mo. Arrows in WT and arrowheads in *Sod1*$^{-/-}$ indicate synaptic cleft. *B*) SSM function. Left panel: RCR, measured from SSM from hindlimb muscle at 20 mo. Middle panel: ATP production from SSM, measured at 20 mo. Right panel: rate of H_2O_2 production from SSM at 20 mo. *C*) NMJ immunofluorescence images from gastrocnemius at 20 mo. Top panels: morphology of postsynaptic AChRs stained with Alexa 488-conjugated α-bungarotoxin. Middle panels: morphology of presynaptic motor neurons in *Thy1* YFP transgenic mice (C57BL/6J background) crossbred to WT and *Sod1*$^{-/-}$ mice. Arrows indicate sprouting and thinning of motor neurons. Bottom panels: overlay images of AChR and motor neuron images shown in top panels. *D*) Rate of denervation score assessment (top panels) and quantification of denervation score at ~18 mo (bottom panel). *E*) Comparison of NMJs in single fibers (top panels) and correlation of fiber diameter and NMJ fragmentation (bottom panel). Arrows indicate NMJs in WT and *Sod1*$^{-/-}$ fibers. *F*) *In situ* isometric contraction properties. Maximum isometric force (top) and specific force (bottom). Values are means ± SE. $^{*}P < 0.05$; $^{\#}P < 0.05$; $^{**}P < 0.01$; $^{***}P < 0.001$. Scale bars = 2 μm (A); 50 μm (*D*)

pears to be occurring on a fiber-by-fiber basis, we also analyzed NMJs in single fibers. As illustrated in Fig. 6*E*, fibers from *Sod1*$^{-/-}$ gastrocnemius muscles exhibited postsynaptic endplates that were considerably fragmented compared to WT endplates. Interestingly, in *Sod1*$^{-/-}$ gastrocnemius at 20 mo, the fiber size/diameter strongly correlated with the fragmentation level of endplates, suggesting innervation of NMJs is a crucial factor in age-associated muscle atrophy. In addition, we tested whether alteration in NMJs leads to functional decline in gastrocnemius muscle. We measured *in situ* isometric contraction using electrical stimulation. When muscles were stimulated by the nerve, force generation was significantly lower for the gastrocnemius muscles of *Sod1*$^{-/-}$ compared to WT mice at both 8 and 20 mo (Fig. 6*F*), a difference that remained when the force was normalized by cross-sectional area (Fig. 6*F*), suggesting that fibers may be functionally denervated.

AChR degeneration in aged *Sod1*$^{-/-}$ muscle

To assess the significance of alterations in the NMJ, we further examined the level of postsynaptic endplates in the gastrocnemius muscle. To quantify fragmentation of the endplates, we analyzed the single-channel confocal *z*-stack images of AChR staining by bungarotoxin. Results demonstrate that in *Sod1*$^{-/-}$ muscle at 18 mo, 80% of the endplates were dispersed and fragmented, as scored by ≥4 segregated "islands"/endplate, while in the WT, only 3% showed fragmentation (**Fig. 7*A***). Not only did the AChRs from *Sod1*$^{-/-}$ muscle show disintegration; they also appeared much smaller in size (Fig. 7*A*). To confirm these observations, we measured the protein and mRNA levels of the AChR-α subunit. It has been reported that in the surgical denervation model, AChR transcript and protein levels increase in response to acute denervation. We have reported previously that transcripts of AChR subunits measured by quantitative real-time PCR were elevated in 10-mo-old *Sod1*$^{-/-}$ compared with WT mice (32). Similar to our previous data, AChR-α mRNA level in aged *Sod1*$^{-/-}$ muscle was ~8 fold higher compared to WT, suggesting that denervation is occurring. However, in contrast to mRNA level, AChR-α protein content was significantly decreased by 60% in *Sod1*$^{-/-}$, meaning that the AChR-α protein level was down-regulated posttranscriptionally. Furthermore, rapsyn, which plays a critical role in clustering of the AChR complex, was significantly declined in aged *Sod1*$^{-/-}$ muscle compared to WT muscle (Fig. 7*C*). Recently, two independent researchers showed that an increase in the Ca^{2+}-dependent cysteine protease, calpain, inhibits AChR-complex clustering by associating with rapsyn in synaptogenesis, as well as in an NMJ disorder, slow channel myasthenia gravis (33). We found that in aged *Sod1*$^{-/-}$ mice, the calpain protein level, as well as activity (data not shown), was significantly elevated at 20 mo of age (Fig. 7*D*). In all, these data support our observation that increased fragmentation of the AChR occurs in aged muscle of *Sod1*$^{-/-}$ mice, which may be associated with a decreased level of AChR at the NMJ.

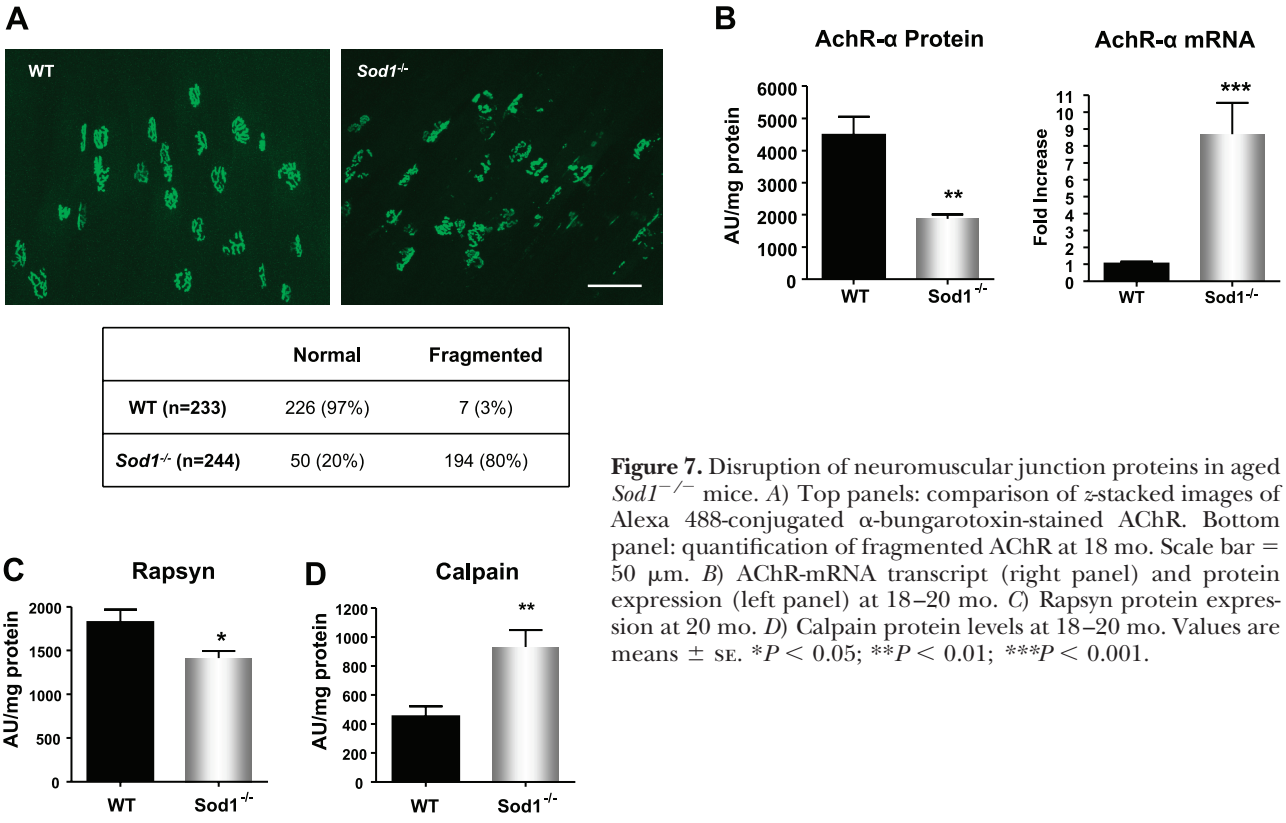

Figure 7. Disruption of neuromuscular junction proteins in aged *Sod1*$^{-/-}$ mice. *A*) Top panels: comparison of *z*-stacked images of Alexa 488-conjugated α-bungarotoxin-stained AChR. Bottom panel: quantification of fragmented AChR at 18 mo. Scale bar = 50 μm. *B*) AChR-mRNA transcript (right panel) and protein expression (left panel) at 18–20 mo. *C*) Rapsyn protein expression at 20 mo. *D*) Calpain protein levels at 18–20 mo. Values are means ± SE. $^{*}P < 0.05$; $^{**}P < 0.01$; $^{***}P < 0.001$.

DISCUSSION

In the present study, we demonstrated that loss of muscle mass in *Sod1*$^{-/-}$ mice is associated with oxidative stress-induced mitochondrial dysfunction and a concomitant increase in myonuclear apoptosis that ultimately result in myofiber atrophy. In addition to the acceleration of muscle atrophy, morphological analysis of muscle from aged *Sod1*$^{-/-}$ mice revealed a conversion of fast glycolytic fibers to slow oxidative fibers. This process is known to be the result of motor-unit remodeling. The selective denervation of muscle fibers, especially type IIb fibers, is followed by reinnervation by axonal sprouting from the adjacent innervated units, leading to a net loss of innervated fibers and functional motor units (8). As a consequence of increased oxidative fibers, there is a considerable increase in mitochondrial density. While it is plausible that mitochondrial biogenesis occurs in response to increased oxidative fibers and increased metabolic demand, the amount of mitochondrial density observed in *Sod1*$^{-/-}$ gastrocnemius is far greater than that seen in predominantly oxidative fibers such as soleus. Moreover, some fibers feature abnormal "giant" mitochondria clusters along the myofibrils, which is similar to defects that are frequently seen in the "ragged red fibers" of mitochondrial myopathy. These observations are supported by a recent report by Dobrowolny *et al.* (34), in which the researchers observed similar swollen, abnormally shaped mitochondria in the muscle-specific *SOD1*^{G93A} mutant mice. These data suggest that the oxidative stress caused by alteration in CuZnSOD level significantly impairs mitochondrial homeostasis. Despite having more mitochondrial content, the overall function of mitochondria from *Sod1*$^{-/-}$ muscle, measured by ATP generation and oxygen consumption, greatly deteriorated with age. There are several possible explanations for increased mitochondrial proliferation in *Sod1*$^{-/-}$ muscle. First, mitochondrial biogenesis genes could be activated by oxidative stress. Previous studies have shown that human fibroblasts treated with H_2O_2 activate peroxisome proliferator-activated receptor-γ coactivator 1α (PGC-1α) and mitochondrial biogenesis genes (35). Interestingly, PGC-1α has been shown to suppress ROS generation and is also required for the induction of ROS-detoxifying enzymes such as GPx1 and MnSOD (36). Our data also confirmed that PGC-1α transcript level was significantly elevated in muscle of *Sod1*$^{-/-}$ mice (Supplemental Fig. S2). Second, because of mitochondrial dysfunction and a deficiency in ATP, muscle cells simply respond as a part of an adaptive measure to increase functional mitochondria to meet the high energy demand of the skeletal muscle. Finally, the mitochondrial proliferation observed in muscle of aged *Sod1*$^{-/-}$ mice could be caused by lack of autophagy to remove oxidatively damaged mitochondria. Consistent with this notion, we found formation of giant mitochondria with large vacuoles and lipid droplets in some of the muscle fibers from *Sod1*$^{-/-}$ muscle, suggestive of lysosomal defects or incomplete macroautophagy (37–38) (Fig. 4*E*). In contrast, other researchers have reported a decrease in mitochondrial content associated with mitochondrial dysfunction with age in sarcopenic muscle (4, 39). In addition, PGC-1α level in skeletal muscle has been shown to decrease during aging (40–41). This suggests that a distinct mechanism of myofiber atrophy may exist in muscle from *Sod1*$^{-/-}$ mice that differs from mechanisms present in normal aging muscle. It is possible that myofibers may undergo a remodeling process in response to high oxidative stress and loss of innervation. In support of this, myocyte enhancing factor 2 (MEF2) transcription factors have been identified as important regulators of myofiber remodeling by interacting with the class II histone deacetylases (HDACs) (42). In a recent study, Cohen *et al.* (43) demonstrated that in response to denervation and also in a mouse model of ALS, HDAC4 controls MEF2-dependent neuromuscular and structural gene expression in myofibers. Further studies are needed to test whether these signaling pathways are activated directly in response to oxidative stress *in vivo*.

We have also demonstrated in this study that mitochondria from aged *Sod1*$^{-/-}$ muscle have higher susceptibility to Ca^{2+}-induced mitochondrial permeability transition pore opening and mitochondria-mediated apoptosis. Single fiber analyses also revealed that the total number of myonuclei was significantly reduced in *Sod1*$^{-/-}$ muscle. It has been suggested that each myonucleus has a limited synthetic capacity and serves a certain cytoplasmic domain and that this domain size remains constant throughout the half-life of the fiber (28). For example, during hypertrophy, new nuclei are brought in by the satellite cells differentiating and fusing to existing fibers to preserve the domain size. Conversely, under a wide variety of conditions leading to muscle atrophy, nuclei are believed to be lost by the apoptotic deletion process (7, 44–45). Thus, the number of nuclei has been considered to be a causative factor in maintaining muscle size (28). However, in a recent report by Bruusgaard *et al.* (46), in which the researchers used *in vivo* time lapse imaging to monitor myonuclei number after denervation injury, very few apoptotic myonuclei were observed, and the researchers argued that most of the apoptosis was occurring in the satellite cells instead of myonuclei. Although we do see extensive denervation in aged *Sod1*$^{-/-}$ muscle, discrepancy between data by Bruusgaard *et al.* (46) and our model could be due to acute damage *vs.* chronic oxidative damage and denervation occurring in *Sod1*$^{-/-}$ muscle fibers. In agreement with our results, other researchers have also reported a similar decrease in myonuclei number in aged mouse skeletal muscle using the single fiber approach (46, 47). As the myonuclei number decreases *via* apoptosis in aged *Sod1*$^{-/-}$ muscle, a simultaneous decrease in fiber diameter takes place, thereby maintaining a nuclear domain constant. We postulate that in *Sod1*$^{-/-}$ muscle, a decrease in myonuclei number significantly limits the ability of muscle cells to synthesize proteins, leading to mito-

chondrial dysfunction and deficiency in overall energy generation. Thus, muscle fibers respond by reducing their size through increased activation of intracellular proteolytic systems as an adaptive mechanism. Indeed, in context with this idea, we observed significant increases in the ubiquitin proteasome system (data not shown) and the cysteine proteases (calpain and caspase-3) that are known to be activated during muscle atrophy. Furthermore, as *Sod1*$^{-/-}$ mice age, chronic oxidative stress may also activate multiple proteolytic pathways to remove oxidatively damaged proteins as a survival mechanism. Notably, more and more evidence points toward ROS as a signaling modulator of the lysosomal autophagic pathway as well as the ubiquitin proteasome system (48–49). The crosstalk between these proteolytic pathways in response to oxidative stress needs further investigation. It is possible that if oxidative damage and a deficiency in energy overwhelm the survival mechanism, the cells undergo apoptosis/necrosis and degenerate, as we have observed in some of the old *Sod1*$^{-/-}$mice.

Another important finding from our study is that the age-dependent muscle atrophy seen in *Sod1*$^{-/-}$ is partially due to age-dependent alteration in neuromuscular innervation and the failure to maintain AChR clusters at the postsynaptic NMJ. We also reported in our previous study that mitochondrial H_2O_2 production correlates strongly with innervation and the degree of muscle atrophy in different models of denervation (13). In the peripheral synapses, H_2O_2, a stable membrane-permeable ROS, has been shown to inhibit the quantal release of acetylcholine and SNAP25, which function in vesicle fusion (50). Recently, Dupuis *et al.* (12) reported that overexpression of uncoupling protein (UCP1) only in the skeletal muscle was enough to dismantle NMJs and trigger distal motor neuron degeneration. These observations imply that increased mitochondrial dysfunction and ROS generation in *Sod1*$^{-/-}$ muscle may be the two critical factors that contribute to the progression of age-related deterioration of NMJs and muscle atrophy. Moreover, it has been well documented that mitochondria play a pivotal role as a Ca^{2+} sink. Cytosolic Ca^{2+} levels are tightly regulated in skeletal muscle for contractile activity, gene expression, and many other functions (51). Disruption of Ca^{2+} homeostasis can have deleterious effects on cell function and can also trigger apoptosis (52). A significant increase in Ca^{2+}-dependent protease calpain observed in our study indirectly supports the hypothesis that the cytosolic Ca^{2+} is elevated in Sod1-null muscle. It has been reported that after denervation injury, mitochondrial Ca^{2+}-retention capacity is significantly reduced (53). In addition, calpain has been shown to play an important role in the clustering of AChR complex by interacting with rapsyn (33). Furthermore, the gene expression of the proteins involved in the maintenance of the NMJs is regulated by 4–6 specialized nuclei that are located adjacent to NMJs, called subsynaptic nuclei (54). On the basis of the anatomical location and our results showing a significant decline in mitochondrial function and increased ROS, these nuclei could also be susceptible to apoptosis, as we demonstrated in this study. Taken together, this series of events may play a critical role in the development of denervation and the acceleration of age-related muscle atrophy observed in *Sod1*$^{-/-}$, as well as in sarcopenia.

This study has provided clear evidence linking oxidative stress-induced mitochondrial dysfunction and denervation in preservation of muscle mass. However, as aging is a complex process and the etiology of sarcopenia most likely involves multiple systems, we cannot rule out the fact that other factors may have synergistic effects on the progression of muscle atrophy in aging. Moreover, in the conventional knockout strategy used to generate our *Sod1*$^{-/-}$ mice, the *Sod1* gene is deleted in every tissue. Therefore, oxidative stress in other tissues may have systemic effects on the skeletal muscle. One prime example is the role of satellite cells and/or other muscle progenitor cells. A large amount of literature has suggested that the regenerative potential of skeletal muscle declines with age and that this impairment is associated with an increase in tissue fibrosis (55–56). A recent study showed that muscle stem cells from aged mice tend to convert from a myogenic to a fibrogenic lineage as they begin to proliferate and that this conversion is mediated by factors in the systemic environment of the old animals (56). Although it has not been well studied, oxidative stress in the microenvironment or the niche of the muscle stem cell may have a deleterious outcome on the regenerative potential of the aged skeletal muscle. Interestingly, our preliminary study shows that there was an increase in TUNEL stain in the satellite cells of *Sod1*$^{-/-}$ fibers, suggesting that satellite cells might be lost due to apoptosis (data not shown). In line with this observation, others have shown that in normal aging, as well as in a surgical denervation model, satellite cell apoptosis was greatly increased (57–58). Currently, studies are under way in our laboratory to address the tissue-specific effect of oxidative stress in age-related muscle loss.

In summary, our findings reveal that chronic oxidative stress due to loss of *Sod1* gene exacerbates muscle atrophy during aging *via* mitochondrial dysfunction, activation of mitochondrial-mediated myonuclear apoptosis, and by altering neuromuscular innervation. We propose that the superoxide-induced NMJ degeneration and mitochondrial dysfunction are one of the potential mechanisms that leads to sarcopenia *in vivo*. FJ

The authors thank Drs. Charles Epstein (University of California, San Francisco, CA, USA) and Ting Ting Huang (Stanford University, Palo Alto, CA, USA) for providing *Sod1*-null breeders, Corinne Price for proofreading our manuscript, and Drs. Asish Chaudhuri, Anson Pierce, James Lechleiter, Walter Ward, and Victoria Frohlich for their input and technical assistance. This work was supported by P01AG020591 (to H.V.R., A.R., S.V.B., L.L.), and a Julie Martin Mid-Career grant from the American Federation for Aging Research (to H.V.R.).

REFERENCES

1. Mansouri, A., Muller, F. L., Liu, Y., Ng, R., Faulkner, J., Hamilton, M., Richardson, A., Huang, T. T., Epstein, C. J., and Van Remmen, H. (2006) Alterations in mitochondrial function, hydrogen peroxide release and oxidative damage in mouse hind-limb skeletal muscle during aging. *Mech. Ageing Dev.* **127,** 298–306
2. Moylan, J. S., and Reid, M. B. (2007) Oxidative stress, chronic disease, and muscle wasting. *Muscle Nerve* **35,** 411–429
3. Choksi, K. B., Nuss, J. E., Deford, J. H., and Papaconstantinou, J. (2008) Age-related alterations in oxidatively damaged proteins of mouse skeletal muscle mitochondrial electron transport chain complexes. *Free Radic. Biol. Med.* **45,** 826–838
4. Figueiredo, P. A., Powers, S. K., Ferreira, R. M., Appell, H. J., and Duarte, J. A. (2009) Aging impairs skeletal muscle mitochondrial bioenergetic function. *J. Gerontol. A Biol. Sci. Med. Sci.* **64,** 21–33
5. Lexell, J., Taylor, C. C., and Sjostrom, M. (1988) What is the cause of the ageing atrophy? Total number, size and proportion of different fiber types studied in whole vastus lateralis muscle from 15- to 83-year-old men. *J. Neurol. Sci.* **84,** 275–294
6. Dupont-Versteegden, E. E. (2005) Apoptosis in muscle atrophy: relevance to sarcopenia. *Exp. Gerontol.* **40,** 473–481
7. Dirks, A. J., and Leeuwenburgh, C. (2004) Aging and lifelong calorie restriction result in adaptations of skeletal muscle apoptosis repressor, apoptosis-inducing factor, X-linked inhibitor of apoptosis, caspase-3, and caspase-12. *Free Radic. Biol. Med.* **36,** 27–39
8. Brooks, S. V., and Faulkner, J. A. (1994) Skeletal muscle weakness in old age: underlying mechanisms. *Med. Sci. Sports. Exerc.* **26,** 432–439
9. Cederna, P. S., Asato, H., Gu, X., van der Meulen, J., Kuzon, W. M., Jr., Carlson, B. M., and Faulkner, J. A. (2001) Motor unit properties of nerve-intact extensor digitorum longus muscle grafts in young and old rats. *J. Gerontol. A Biol. Sci. Med. Sci.* **56,** B254–B258
10. Balice-Gordon, R. J. (1997) Age-related changes in neuromuscular innervation. *Muscle Nerve Suppl.* **5,** S83–S87
11. Lysakowski, A., Figueras, H., Price, S. D., and Peng, Y. Y. (1999) Dense-cored vesicles, smooth endoplasmic reticulum, and mitochondria are closely associated with non-specialized parts of plasma membrane of nerve terminals: implications for exocytosis and calcium buffering by intraterminal organelles. *J. Comp. Neurol.* **403,** 378–390
12. Dupuis, L., Gonzalez de Aguilar, J. L., Echaniz-Laguna, A., Eschbach, J., Rene, F., Oudart, H., Halter, B., Huze, C., Schaeffer, L., Bouillaud, F., and Loeffler, J. P. (2009) Muscle mitochondrial uncoupling dismantles neuromuscular junction and triggers distal degeneration of motor neurons. *PLoS One* **4,** e5390
13. Muller, F. L., Song, W., Jang, Y., Liu, Y., Sabia, M., Richardson, A., and Van Remmen, H. (2007) Denervation-induced skeletal muscle atrophy is associated with increased mitochondrial ROS production. *Am. J. Physiol.* **293,** R1159–R1168
14. Elchuri, S., Oberley, T. D., Qi, W., Eisenstein, R. S., Jackson Roberts, L., Van Remmen, H., Epstein, C. J., and Huang, T. T. (2005) CuZnSOD deficiency leads to persistent and widespread oxidative damage and hepatocarcinogenesis later in life. *Oncogene* **24,** 367–380
15. Muller, F., Song, W., Liu, Y. H., Qi, W. B., Strong, R., Roberts, L. J., Chaudhuri, A., Faulkner, J., Huang, T. T., Epstein, C., Richardson, A., and Van Remmen, H. (2005) Absence of Cu, Zn-Sod causes severe oxidative stress and acceleration of age-dependent skeletal muscle atrophy. *Free Rad. Biol. Med.* **39,** S127–S127
16. Bhattacharya, A., Muller, F. L., Liu, Y., Sabia, M., Liang, H., Song, W., Jang, Y. C., Ran, Q., and Van Remmen, H. (2009) Denervation induces cytosolic phospholipase A2-mediated fatty acid hydroperoxide generation by muscle mitochondria. *J. Biol. Chem.* **284,** 46–55
17. Muller, F. L., Liu, Y., and Van Remmen, H. (2004) Complex III Releases superoxide to both sides of the inner mitochondrial membrane. *J. Biol. Chem.* **279,** 49064–49073
18. Pagliari, L. J., Kuwana, T., Bonzon, C., Newmeyer, D. D., Tu, S., Beere, H. M., and Green, D. R. (2005) The multidomain proapoptotic molecules Bax and Bak are directly activated by heat. *Proc. Natl. Acad. Sci. U. S. A.* **102,** 17975–17980
19. Newmeyer, D. D., Farschon, D. M., and Reed, J. C. (1994) Cell-free apoptosis in *Xenopus* egg extracts: inhibition by Bcl-2 and requirement for an organelle fraction enriched in mitochondria. *Cell* **79,** 353–364
20. Saelim, N., Holstein, D., Chocron, E. S., Camacho, P., and Lechleiter, J. D. (2007) Inhibition of apoptotic potency by ligand stimulated thyroid hormone receptors located in mitochondria. *Apoptosis* **12,** 1781–1794
21. Wada, K. I., Katsuta, S., and Soya, H. (2003) Natural occurrence of myofiber cytoplasmic enlargement accompanied by decrease in myonuclear number. *Jpn. J. Physiol.* **53,** 145–150
22. Wada, K. I., Takahashi, H., Katsuta, S., and Soya, H. (2002) No decrease in myonuclear number after long-term denervation in mature mice. *Am. J. Physiol. Cell Physiol.* **283,** C484–C488
23. Schaefer, A. M., Sanes, J. R., and Lichtman, J. W. (2005) A compensatory subpopulation of motor neurons in a mouse model of amyotrophic lateral sclerosis. *J. Comp. Neurol.* **490,** 209–219
24. Burkholder, T. J., Fingado, B., Baron, S., and Lieber, R. L. (1994) Relationship between muscle fiber types and sizes and muscle architectural properties in the mouse hindlimb. *J. Morphol.* **221,** 177–190
25. Okado-Matsumoto, A., and Fridovich, I. (2001) Subcellular distribution of superoxide dismutases (SOD) in rat liver Cu, Zn-SOD in mitochondria. *J. Biol. Chem.* **276,** 38388–38393
26. Powers, S. K., and Jackson, M. J. (2008) Exercise-induced oxidative stress: cellular mechanisms and impact on muscle force production. *Physiol. Rev.* **88,** 1243–1276
27. Kagan, V. E., Borisenko, G. G., Tyurina, Y. Y., Tyurin, V. A., Jiang, J., Potapovich, A. I., Kini, V., Amoscato, A. A., and Fujii, Y. (2004) Oxidative lipidomics of apoptosis: redox catalytic interactions of cytochrome *c* with cardiolipin and phosphatidylserine. *Free Radic. Biol. Med.* **37,** 1963–1985
28. Allen, D. L., Roy, R. R., and Edgerton, V. R. (1999) Myonuclear domains in muscle adaptation and disease. *Muscle Nerve* **22,** 1350–1360
29. Shefner, J. M., Reaume, A. G., Flood, D. G., Scott, R. W., Kowall, N. W., Ferrante, R. J., Siwek, D. F., Upton-Rice, M., and Brown, R. H., Jr. (1999) Mice lacking cytosolic copper/zinc superoxide dismutase display a distinctive motor axonopathy. *Neurology* **53,** 1239–1246
30. Flood, D. G., Reaume, A. G., Gruner, J. A., Hoffman, E. K., Hirsch, J. D., Lin, Y. G., Dorfman, K. S., and Scott, R. W. (1999) Hindlimb motor neurons require Cu/Zn superoxide dismutase for maintenance of neuromuscular junctions. *Am. J. Pathol.* **155,** 663–672
31. Feng, G., Mellor, R. H., Bernstein, M., Keller-Peck, C., Nguyen, Q. T., Wallace, M., Nerbonne, J. M., Lichtman, J. W., and Sanes, J. R. (2000) Imaging neuronal subsets in transgenic mice expressing multiple spectral variants of GFP. *Neuron* **28,** 41–51
32. Kostrominova, T. Y., Pasyk, K. A., Van Remmen, H., Richardson, A. G., and Faulkner, J. A. (2006) Adaptive changes in structure of skeletal muscles from adult Sod1 homozygous knockout mice. *Cell Tissue Res.* **327,** 595–605
33. Chen, F., Qian, L., Yang, Z. H., Huang, Y., Ngo, S. T., Ruan, N. J., Wang, J., Schneider, C., Noakes, P. G., Ding, Y. Q., Mei, L., and Luo, Z. G. (2007) Rapsyn interaction with calpain stabilizes AChR clusters at the neuromuscular junction. *Neuron* **55,** 247–260
34. Dobrowolny, G., Aucello, M., Rizzuto, E., Beccafico, S., Mammucari, C., Bonconpagni, S., Belia, S., Wannenes, F., Nicoletti, C., Del Prete, Z., Rosenthal, N., Molinaro, M., Protasi, F., Fano, G., Sandri, M., and Musaro, A. (2008) Skeletal muscle is a primary target of SOD1G93A-mediated toxicity. *Cell Metab.* **8,** 425–436
35. Lee, H. C., and Wei, Y. H. (2005) Mitochondrial biogenesis and mitochondrial DNA maintenance of mammalian cells under oxidative stress. *Int. J. Biochem. Cell Biol.* **37,** 822–834
36. St-Pierre, J., Drori, S., Uldry, M., Silvaggi, J. M., Rhee, J., Jager, S., Handschin, C., Zheng, K., Lin, J., Yang, W., Simon, D. K., Bachoo, R., and Spiegelman, B. M. (2006) Suppression of reactive oxygen species and neurodegeneration by the PGC-1 transcriptional coactivators. *Cell* **127,** 397–408
37. Terman, A., and Brunk, U. T. (2006) Oxidative stress, accumulation of biological 'garbage', and aging. *Antioxid. Redox Signal.* **8,** 197–204

38. Terman, A., Gustafsson, B., and Brunk, U. T. (2006) The lysosomal-mitochondrial axis theory of postmitotic aging and cell death. *Chem. Biol. Interact.* **163,** 29–37
39. Lyons, C. N., Mathieu-Costello, O., and Moyes, C. D. (2006) Regulation of skeletal muscle mitochondrial content during aging. *J. Gerontol. A Biol. Sci. Med. Sci.* **61,** 3–13
40. Wenz, T., Rossi, S. G., Rotundo, R. L., Spiegelman, B. M., and Moraes, C. T. (2009) Increased muscle PGC-1α expression protects from sarcopenia and metabolic disease during aging. *Proc. Natl. Acad. Sci. U. S. A.* **106,** 20405–20410
41. Anderson, R., and Prolla, T. (2009) PGC-1α in aging and anti-aging interventions. *Biochim. Biophys. Acta.* **1790,** 1059–1066
42. Potthoff, M. J., Olson, E. N., and Bassel-Duby, R. (2007) Skeletal muscle remodeling. *Curr. Opin. Rheumatol.* **19,** 542–549
43. Cohen, T. J., Barrientos, T., Hartman, Z. C., Garvey, S. M., Cox, G. A., and Yao, T. P. (2009) The deacetylase HDAC4 controls myocyte enhancing factor-2-dependent structural gene expression in response to neural activity. *FASEB J.* **23,** 99–106
44. Siu, P. M., Pistilli, E. E., and Alway, S. E. (2005) Apoptotic responses to hindlimb suspension in gastrocnemius muscles from young adult and aged rats. *Am. J. Physiol. Regul. Integr. Comp. Physiol.* **289,** R1015–R1026
45. Adhihetty, P. J., O'Leary, M. F., Chabi, B., Wicks, K. L., and Hood, D. A. (2007) Effect of denervation on mitochondrially mediated apoptosis in skeletal muscle. *J. Appl. Physiol.* **102,** 1143–1151
46. Bruusgaard, J. C., Liestol, K., and Gundersen, K. (2006) Distribution of myonuclei and microtubules in live muscle fibers of young, middle-aged, and old mice. *J. Appl. Physiol.* **100,** 2024–2030
47. Brack, A. S., Bildsoe, H., and Hughes, S. M. (2005) Evidence that satellite cell decrement contributes to preferential decline in nuclear number from large fibres during murine age-related muscle atrophy. *J. Cell Sci.* **118,** 4813–4821
48. Scherz-Shouval, R., and Elazar, Z. (2007) ROS, mitochondria and the regulation of autophagy. *Trends Cell Biol.* **17,** 422–427
49. Li, Y. P., Chen, Y., Li, A. S., and Reid, M. B. (2003) Hydrogen peroxide stimulates ubiquitin-conjugating activity and expression of genes for specific E2 and E3 proteins in skeletal muscle myotubes. *Am. J. Physiol. Cell Physiol.* **285,** C806–C812
50. Giniatullin, A. R., Darios, F., Shakirzyanova, A., Davletov, B., and Giniatullin, R. (2006) SNAP25 is a pre-synaptic target for the depressant action of reactive oxygen species on transmitter release. *J. Neurochem.* **98,** 1789–1797
51. Brookes, P. S., Yoon, Y., Robotham, J. L., Anders, M. W., and Sheu, S. S. (2004) Calcium, ATP, and ROS: a mitochondrial love-hate triangle. *Am. J. Physiol. Cell Physiol.* **287,** C817–C833
52. Giorgi, C., Romagnoli, A., Pinton, P., and Rizzuto, R. (2008) Ca^{2+} signaling, mitochondria and cell death. *Curr. Mol. Med.* **8,** 119–130
53. Csukly, K., Ascah, A., Matas, J., Gardiner, P. F., Fontaine, E., and Burelle, Y. (2006) Muscle denervation promotes opening of the permeability transition pore and increases the expression of cyclophilin D. *J. Physiol.* **574,** 319–327
54. Grady, R. M., Starr, D. A., Ackerman, G. L., Sanes, J. R., and Han, M. (2005) Syne proteins anchor muscle nuclei at the neuromuscular junction. *Proc. Natl. Acad. Sci. U. S. A.* **102,** 4359–4364
55. Conboy, I. M., Conboy, M. J., Wagers, A. J., Girma, E. R., Weissman, I. L., and Rando, T. A. (2005) Rejuvenation of aged progenitor cells by exposure to a young systemic environment. *Nature* **433,** 760–764
56. Brack, A. S., Conboy, M. J., Roy, S., Lee, M., Kuo, C. J., Keller, C., and Rando, T. A. (2007) Increased Wnt signaling during aging alters muscle stem cell fate and increases fibrosis. *Science* **317,** 807–810
57. Jejurikar, S. S., Marcelo, C. L., and Kuzon, W. M., Jr. (2002) Skeletal muscle denervation increases satellite cell susceptibility to apoptosis. *Plast. Reconstr. Surg.* **110,** 160–168
58. Bruusgaard, J. C., and Gundersen, K. (2008) In vivo time-lapse microscopy reveals no loss of murine myonuclei during weeks of muscle atrophy. *J. Clin. Invest.* **118,** 1450–1457

Received for publication September 21, 2009.
Accepted for publication December 3, 2009.